Proceedings of the ASME 2025 44th International Conference on Ocean, Offshore and Arctic Engineering
OMAE2025
June 22-27, 2025, Vancouver, British Columbia, Canada

OMAE2025-156756

TANKER HULL IN REGULAR WAVES: CFD COMPARISON TO EXISTING EXPERIMENTS

Cedric Fallet[1,*], Tobias Lampe[1], Marco Klein[1], Sören Ehlers[1]

[1]German Aerospace Center (DLR), Institute for Maritime Energy Systems

ABSTRACT

The evaluation of a ship's performance in seaways is crucial for its efficient operation including passenger comfort and fatigue strength. With growing computing power, proper CFD predictions become increasingly attractive. During the EU project "Extreme Seas" an extensive experimental test campaign with a model of a chemical tanker has been conducted. In this paper, the motion of the vessel in regular waves within the Stokes-II regime are assessed by means of CFD-Simulation and compared to the experimental results. Moreover, the influence of the surge motion on the overall ship response is investigated by conducting the simulations with two enabled degrees of freedom as well as with a spring system to additionally enable surge motions and reproduce the experimental setup. Comparison to experimental data is performed by means of response amplitude operators for heave and pitch. The simulations show a reasonable agreement with the experimental results for both investigated numerical setups. However, the CFD results indicate that a restricted surge motion leads to an overestimation of the pitch response for long waves up to the peak of the response amplitude operator. In contrast to that, the heave motion is barely influenced by the surge motion. These findings are scrutinized through application of the Boundary Element Method confirming the potential accuracy improvement when including surge motions in the seakeeping simulations.

Keywords: CFD, seakeeping, wave-structure interactions

1. INTRODUCTION

Naval hydrodynamics is on its way towards full scale numerical predictions considering complete sea trials as well as harsh seakeeping conditions [1, 2]. Still, an integral part is the validation of the numerical approaches [3, 4]. This commonly poses several challenges, e.g. due to limited availability of full-scale data or the violation of scaling laws for model-scale experiments. However, the latter issue becomes negligible for seakeeping investigations at model scale where inertia forces dominate and friction effects turn irrelevant (i.e. no flow separation) which is the case for straight heading and moderate wave steepness. Especially Computational Fluid Dynamics (CFD) can theoretically circumvent such limitations allowing the replication and assessment of numerical model tests at arbitrary scales. With the rise of computational power and evolution of CFD algorithms, CFD is applied to vast range of maritime problems from propeller performance and hull optimization to full manoeuvre simulations [3, 5, 6]. For the evaluation of a ship's seakeeping behaviour, reduced order methods based on potential theory are well established. However, in contrast to most of these models, CFD is able to cover also steep waves, their nonlinear effects and the influence of friction [7, 8], which increases fidelity and reliability of the results for a wide range of real wave phenomena.

In the present work, the commercial CFD code *Star-CCM+* [9] is utilized for the assessment of the seakeeping performance and its comparison to the experimental data. The work provides RANS simulation results and corresponding experimental data for the motion of a chemical tanker (CT) in regular head waves. The full range of the experimental results has been presented in [10] and the corresponding tanker geometry has been part of the extended CFD study in [11]. Within this paper, two numerical modelling approaches with increasing complexity are used to recreate the experimental setup and investigate the influence on the simulated results. In the referenced experiments, the ship is connected to a spring-pendulum system which allows surge motions to a certain extend. However, the restriction of the surge motion is a regularly applied approach in CFD when simulating head waves. Therefore, the effect of the surge motions of the ship on the predicted heave and pitch motion is assessed. In general, a sufficiently accurate ship response in head waves can be obtained by fixing all motions except heave and pitch motions [12–14]. This procedure assumes a negligible effect of the surge motion and allows to simplify the numerical setup as no artificial restoring force for the surge motion has to be applied to prevent a constant drift of the ship. Nevertheless, for waves with increasing wave lengths the surge motion and thus its potential influence on the overall ship response increases as well. For the investigation of the influence of the surge motion and its restriction, two numer-

*Corresponding author: cedric.fallet@dlr.de

ical setups are utilized that decrease the abstraction level of the experimental setup. First, the standard approach is implemented, which prohibits any surge motions during the simulation. Secondly, the ship is connected to a simple spring that fixes the ship's average position but enables surge motions. The findings of the comparison of these two setups are confirmed by means of the Boundary Element Method (BEM). For that, the wave excitation forces and radiation force from the BEM solver *NEMOH* [15–17] are taken to solve the motion equations in the frequency-domain with and without a restricted surge amplitude.

To sum up, the authors aim to provide a paper showcasing CFD and experimental results for the chemical tanker in regular head waves including an assessment of the influence of the surge motion on heave and pitch.

2. EXPERIMENTAL SETUP

The experiments were conducted at Technical University of Berlin's seakeeping basin and have been published in [10]. The basin has the following dimensions: length 110 m, width 8 m, depth 1 m and is equipped with a wave generator operating in piston mode and a wave damping slope to mitigate reflections. The model was free to heave and pitch, while the surge motion was bound to an elastic suspension system consisting of a spring connected via strings to a counter weight on a pendulum. Due to the employed suspension system, the ship is still able to conduct surge motions but restricted in its amplitude. During the experiment, the model was kept at zero speed and exposed to head waves. Measurements involved the ship motion, the vertical bending moment (vbm), the green water height on deck and slamming pressures at bow and stern. The lines drawing of the chemical tanker is depicted in Fig. 1, whereas Table 1 shows the main dimensions of the ship.

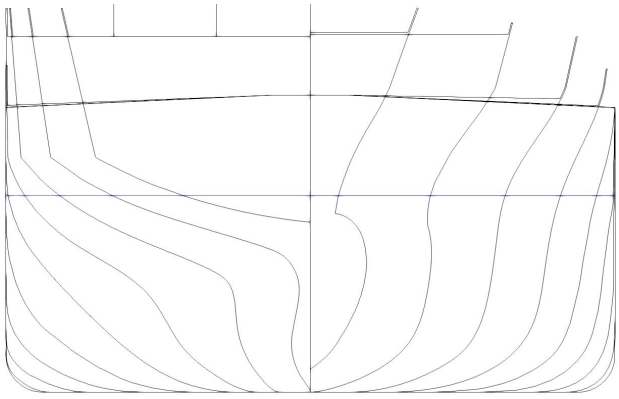

FIGURE 1: LINES DRAWING OF USED CT GEOMETRY, 20 FRAMES BETWEEN AP AND FP. STILL WATER SURFACE INDICATED IN BLUE.

The ship has been investigated in regular waves as well as transient wave packets (TWPs). The TWPs (refer e.g. to [18]) are individually customised wave groups in terms of an amplitude spectrum of a certain shape and bandwidth, as well as manipulated phases. TWPs represent an efficient approach for seakeeping tests as they allow the analysis of the system behaviour for various frequencies, e.g. RAOs, within a single test run. On the opposite,

TABLE 1: MAIN PARTICULARS OF THE CHEMICAL TANKER

Quantity	Abbreviation	Unit	Ship	Model
Length over all	L_{oa}	[m]	170	2.428
Length btw. perp.	L_{pp}	[m]	161	2.300
Breadth moulded	B	[m]	28	0.400
Draft	T	[m]	9	0.129
Displacement	Δ	[t]	30666	0.0894
Scale	λ_s	[-]	1	70

following the conventional approach, a large number of regular waves of varying frequency is necessary to obtain the RAOs. Further details can be found in [10] and a thorough assessment of the TWPs is given e.g. in [19].

2.1 Suspension system

The suspension system which was harnessed during the experiments consists of a spring in front of the ship and a pendulum behind the ship's stern. The mass of the pendulum and the spring are not directly connected to the ship. Instead, the forces of the pendulum and the spring are exerted via two diverging strings that are connected to a beam which is then joint with the ship through a bearing near the ship's center of gravity (cf. Fig. 2). By deflection of the pendulum the spring is tensioned prior to a test run to retain the ship's average position during the test. This setup permits surge motions of the ship while the influence on the other degrees of freedom is relatively small. However, the surge motion itself depends on the spring characteristics and the dynamics of the pendulum. A schematic overview of the described suspension system is shown in Fig. 3. Not all details of the geometric extent of the setup are documented, giving some freedom when implementing a suited substitution model for the simulations.

3. METHODS

A state of the art RANS approach is applied within a commercial Finite-Volume CFD solver to predict the unsteady seakeeping behaviour of a ship in head waves. Using the Einstein convention and tensor notation, the fundamental equations are defined by the Navier-Stokes equations, which are given here in their Reynolds-averaged form. They consist of mass

$$\frac{\partial \rho}{\partial t} + \frac{\partial (\rho \bar{u}_i)}{\partial x_i} = 0 \tag{1}$$

and momentum conservation

$$\frac{\partial (\rho \bar{u}_i)}{\partial t} + \frac{\partial}{\partial x_j}\left(\rho \bar{u}_i \bar{u}_j + \overline{u_i' u_j'}\right) = -\frac{\partial \bar{p}}{\partial x_i} + \frac{\partial \bar{\tau}_{ij}}{\partial x_j}. \tag{2}$$

Here, ρ denotes fluid density, t time, u velocity, x position and p pressure. τ depicts the viscous stress tensor. The RANS equations are closed by a linear, two-equations k-ω-turbulence model frequently utilized for simulations in the naval context [3]. In addition to solution methods solely for the RANS equations, the simulation of a ship hull in waves requires several other modelling

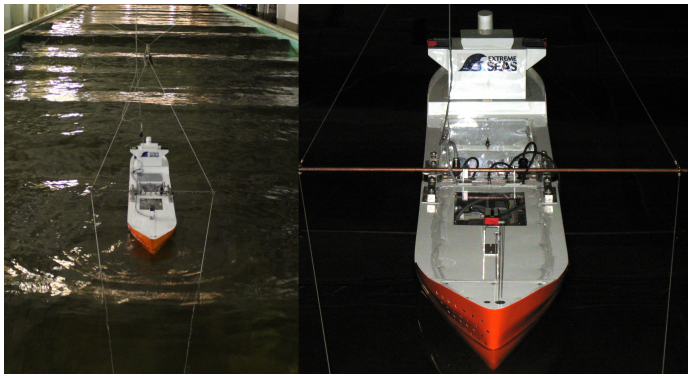

FIGURE 2: CHEMICAL TANKER MODEL AND ITS CONNECTION TO THE SUSPENSION SYSTEM.

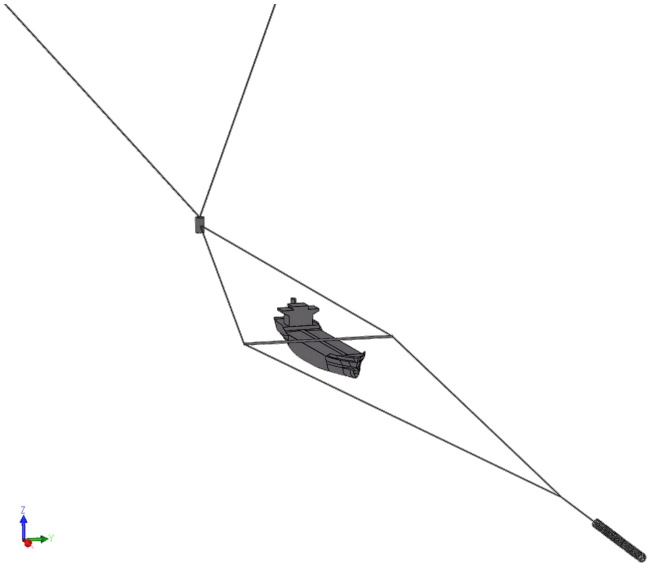

FIGURE 3: SCHEMATIC VISUALIZATION OF THE SUSPENSION SYSTEM USED IN THE EXPERIMENTS.

approaches. An important cornerstone is a proper formulation for a two phase flow including a well resolved interface between the liquid water phase and the air. Besides that, the motions of the ship or hull need to be incorporated in the numerical setup. Further relevant aspects include wave generation, treatment of the boundary conditions and in particular mechanisms to reduce artificial reflections of disturbances at these boundaries.

3.1 Modelling the two phase flow

The two main approaches to model multiple phases mostly differ in their reconstruction of the interface between phases. While interface-tracking methods directly solve for the position of the surface between phases, volume based methods like the well established Volume of Fluid (VoF) method utilize scalar field functions. The VoF approach is particularly suited for the standard CFD algorithms but allows only an indirect identification of the location of the interface [20]. The applied VoF-method solves an additional transport equation for the volume fraction α_i for $n-1$ phases where n represents the number of all modelled phases (here: $n = 2$). The transport equation is given by

$$\frac{\partial \alpha_i}{\partial t} + \nabla \cdot (\alpha_i \mathbf{v}) = 0 \,, \tag{3}$$

while the volume fraction of the last phase can be obtained from

$$\sum_{i=1}^{n} \alpha_i = 1 \,. \tag{4}$$

The volume fraction defines the amount of volume which is occupied in every cell by the specific phase. Therefore, regions filled with a single phase contain only cells with a volume fraction of one for the respective phase and zero for the remaining phases. Thus, the interface is characterized by a volume fraction ranging between $0.0 \leq \alpha_i \leq 1.0$. At this phase interface, the fluid properties are taken based on the mixture of the phases. In order to achieve an accurate solution, an adequate mesh resolution at the interface is required. Additionally, special numerical schemes are needed to obtain a sharp edge between the phases, as the interface tends to be smeared. In this case, the High Resolution Interface Capturing (HRIC) scheme is applied to maintain a clearly defined separation of the respective phases [21]. The HRIC scheme adapts the spatial discretization schemes for the equations for the volume fraction, as the common upwind or central schemes are not well suited for the characteristics of the additional transport equations for the volume fraction [22].

3.2 Integration of rigid body motions

The motions of the ship are defined by the six equations of motion covering three translational and three rotational degrees of freedom (DOF). In the current work, only the pitch, heave and the surge DOF are considered. These equations are coupled to the RANS equations through the body forces acting on the ship and vice versa. In order to implement the body motions in the simulation, multiple approaches are known, which either deform the mesh according to the movement of the body or rigidly move the whole mesh. Due to its high flexibility, the overset mesh approach is well suited for a wide range of motion related problems such as seakeeping simulations. The main idea is to make use of a static background mesh covering the total flow domain and an additional overset mesh for the flow domain bound to the moving body. This additional mesh is directly connected to the motions

of the body and thus moves relatively to the static background mesh. The key for the overset mesh approach is an accurate interpolation of the flow quantities between the two meshes since only one mesh at a time is active in regions where the two meshes overlap. The quantities at the edge of the overset mesh need to be transferred either to the background mesh or from background mesh to the overset mesh. This usually implies some restrictions for the maximum time step and the mesh resolution at these locations. So a critical part are the cell sizes at the interface of overset and background mesh that have to be of similar size in order to achieve a proper interpolation quality. This requires a priori estimation of the ship motions to utilize proper mesh refinements or an automated, adaptive mesh refinement procedure like it is provided in *Star-CCM+*. Despite these restrictions, the overset grid approach is well established for seakeeping simulations, both for its flexibility and high efficiency compared to approaches requiring continuous remeshing due to direct mesh deformations [13, 23].

3.3 Wave generation and boundary conditions

In order to generate a desired wave in the numerical flow domain, the associated flow variables velocity, pressure and water volume fraction can directly be imposed at the boundaries of the flow domain. This requires specification of the time-varying flow quantities which can be obtained from wave theories but also from external methods like potential flow solvers. In this study, the required boundary values are computed internally through a proper nonlinear wave theory. Although small water waves are well approximated by linear wave theories, the wave parameters utilized in these investigations lead to waves, whose nonlinear behaviour is not negligible, therefore requiring nonlinear wave theory for their description [24, 25]. A well established approach for that is the fifth order Stokes theory based on a Fourier expansion of the velocity potential around the dimensionless wave steepness [26, 27]. Fifth order Stokes theory was already successfully applied for wave generation in CFD for waves not conforming to linear wave theory. As it can be seen from Fig. 7, higher order Stokes theories are applicable for steeper waves and also smaller water depths than linear wave theory which makes it favorable when investigating wider ranges of wave parameters. In *Star-CCM+* it is possible to impose boundary conditions for waves based on fifth order Stokes theory, which is used to prescribe specific wave characteristics at the inlet of the domain and also to enforce these in certain regions [28]. The forcing of the solution towards simpler analytic solutions is an important key to significantly reduce the required domain size. For the sake of computational efficiency the boundaries need to be placed near the flow of interest, although this increases the spurious influence of the boundaries e.g due to numerical reflections. In order to reduce their influence, various approaches ranging from the implementation of numerical beaches, porous media to artificial source terms are known. One approach is the mentioned forcing towards an analytic solution, that is provided by the utilized CFD code. The idea is to define a forcing zone in which a source term is added to the momentum equations. The source term is defined by:

$$q_{f,i} = b_i\left(\vec{x}\right)\rho_i\left(W_i - W_i^*\right) \tag{5}$$

where W_i is the velocity in one of the spatial directions at cell i, W_i^* is the analytical solution, ρ_i the density and b_i is a smoothly varying function in space that scales the strength of the forcing source term. By penalizing deviations from the analytical solution towards the boundaries and using the analytical solution simultaneously as the boundary condition, reflections can be significantly reduced. All the conducted simulations rely solely on this forcing approach.

For the sake of brevity, well-known fundamental equations are omitted here. Interested readers are referred e.g. to [29] for CFD in general and e.g. to [3, 30] for maritime aspects. In the following, specific details on the numerical setup will be presented.

4. NUMERICAL SETUP

Although the numerical setups depend on the specific case defined by the respective wave parameters, the base settings are presented in the following. These are in line with best-practice recommendations in the literature [13], guidelines e.g by the International Towing Tank Conference (*ITTC*) [31] and the *Star-CCM+* software user guide [28].

4.1 Flow domain and boundary conditions

The boundary conditions of the flow domain are chosen according to [31]. A standard velocity based inflow condition together with a pressure-based outflow condition is imposed at inlet and outlet. The bottom boundary condition is given by a no-slip wall, while the boundary at the top is also defined as an inflow condition. As the flow problem is symmetric to the x-z-plane (according to the coordinate system with positive x-axis from stern to bow, y-axis to portside and z-axis from keel to deck), a symmetry condition is used for the side boundary located at midship. For the remaining side boundary, a velocity inlet condition is utilized, although other options like a slip-wall condition or symmetry condition might be feasible as well. All the applied boundary conditions are also highlighted in Fig. 4 and Fig. 5. The locations of the boundaries fulfill the minimum requirements given in [31] and depend on the simulated wave length. The domain is enlarged with increasing wave lengths in order to minimize the influence of the boundaries on the flow around the ship. By application of the forcing approach, emitted disturbances are damped towards the lateral and longitudinal boundaries of the domain. For all simulations, the forcing technique is applied at the inflow and outflow boundary, as well as the side boundary. The length of the forcing zones is at least 1.5 wave lengths normal to inflow and outflow boundary ($L_{forcing} = 1.5\lambda$) and $1.0L_{pp}$ normal to the side boundary ($L_{forcing,\,side} = 1.0L_{pp}$). Here, L_{pp} and λ denote ship length between perpendiculars and wave length, respectively. The domain extent is then chosen in such a way that there is a minimum distance between the forcing zone and the ship which is called here the buffer zone. The buffer zones are chosen rather large with $L_{buffer} = 1.0\lambda$ and $L_{buffer,\,side} = 1.0L_{pp}$ preventing influence on the flow of interest as the flow can develop undisturbed towards its physical state. The extent of the forcing zones and buffer zones are visualized in Fig. 4, while Fig. 5 shows the domain extends (distance W to the side boundary shown in Fig. 4), whose definitions are summarized in Tab. 2.

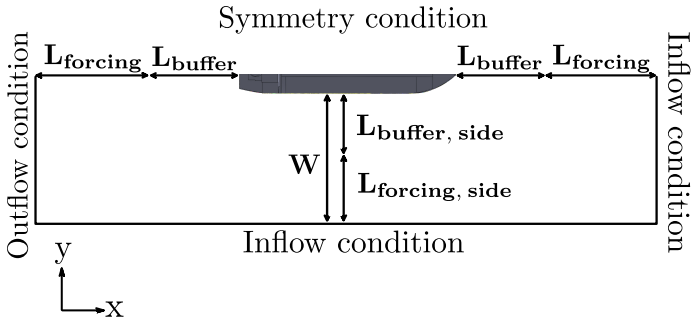

FIGURE 4: OVERVIEW ON THE FORCING AND BUFFER ZONE LENGTHS AND APPLIED BOUNDARY CONDITIONS

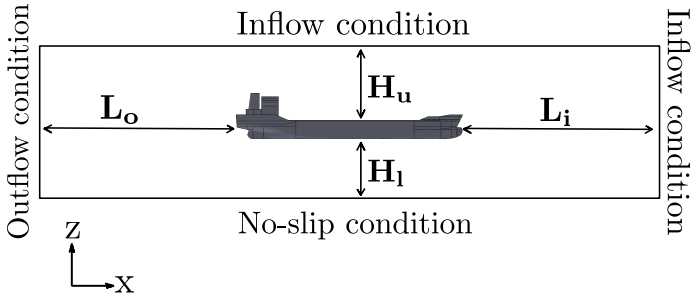

FIGURE 5: OVERVIEW ON THE COMPUTATIONAL DOMAIN EXTENTS AND APPLIED BOUNDARY CONDITIONS

The distance to the bottom boundary is defined by the depth of the model basin d and the ship's draft.

TABLE 2: DIMENSIONS OF FLOW DOMAIN

Dimension	Size
H_u	L_{pp}
H_l	$d - T$
W	$2.0\,L_{pp}$
L_i	$\max(2.0\,L_{pp}, 2.5\,\lambda)$
L_o	$\max(2.5\,L_{pp}, 2.5\,\lambda)$

4.2 Mesh

The discretization of the domain, the mesh, is a hexahedron dominated, unstructured, trimmed mesh that is adapted to specific waves through various local refinements. Especially the free surface requires a high mesh resolution to accurately capture the interface between water and air as well as the large gradients in this region. General guidelines for the resolution of the mesh at the free surface suggest to use a certain number of cells per wave length and per wave height. For all waves, the number of cells is set to 20 per wave height and 80-100 per wave length following recommendations given in [28]. To account for the exponential decay of the wave motions additional refinements along the vertical axis are placed below the mean waterline reaching to depths where the particle velocity is reduced by a factor of two, four and eight. The mesh refinements around the ship aim for a proper

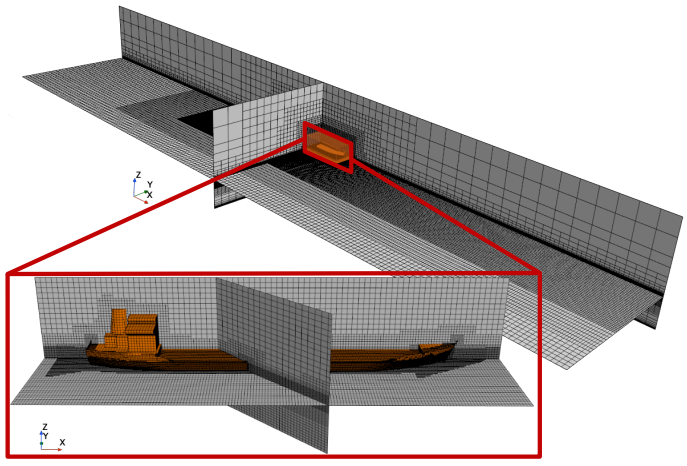

FIGURE 6: CHARACTERISTIC BACKGROUND AND OVERSET MESH

mesh resolution around more complex geometrical parts of the ship like the stern and the bow. The influence of the friction on the seakeeping behaviour is assumed to be small so that the boundary layer does not need to be fully resolved. Because of that, only a small number of prismatic cell layers is generated at the wetted ship surface, whose size is approximated by the wave celerity and an y+ value of around 80. Besides these physics based refinements, further refinements are present at the overlap region of the background mesh and the overset mesh in order to ensure a sufficient interpolation quality in the overset approach. Figure 6 shows a representative mesh consisting of background and overset mesh covering the total domain, including a more detailed view of the overset mesh. The combined number of cells from overset and background mesh is mainly depending on the wave length but it ranges from 3.1 millions for the longest simulated wave to 5.1 millions for the shortest simulated wave. It should be noted that these number do not directly refer to the total number of active cells as the overset approach implies on-the-fly activation/deactivation of cells leading to an effective number of cells which is reduced by around one million.

4.3 Numerical schemes

For the solution process, a SIMPLE algorithm is applied that semi-implicitly solves the momentum equations, a pressure-correction as well as additional equations, e.g. for the turbulence model in a segregated manner [32]. Convective flux terms are evaluated through a second order scheme, whereas the gradients required for the viscous flux terms are approximated by the Least-Squares approach. A second order Backward Differentiation Formula (BDF) is utilized as a time integration scheme for a time accurate flow solution. The time step for temporal evolution has to be chosen according to the discretization schemes and in conformity with the CFL condition. For second order time integration schemes, Courant number should not be higher than 0.5 in simulations with free surface according to [28] and preferably even below 0.25. In general, the time step needs to be small enough to resolve the physical phenomena of interest which for simulations of a ship in regular waves implies at least a suitable

temporal resolution of the wave period T_w. In practice, the time step is set to at most $\Delta t = \frac{T_w}{1000}$, which is smaller than the usual recommendations given e.g in [28] or given by *ITTC* but allowed to maintain a lower discretization error over the total duration of the simulation. Especially, the recommendation to set $\Delta t = \frac{T_w}{100}$ proposed in [31], is too high for our specific test case to preserve a stable and accurate resolution of the free surface. It was found that an important factor for the restrictive time step size is the limited water depth of only 70m in real scale.

4.4 Wave parameters

For the determination of the RAOs for the heave and pitch motion and the assessment of the influence of the surge motion on them, six regular waves from the Stokes-II domain are chosen. From these, four are part of the model test and they range from $\frac{\lambda}{L_{pp}} = 0.8$ to 2.6. The specific wave parameters prescribed at the boundary conditions and given as initial condition are defined in Tab. 3. In this, λ is the wave length and ω and H denote wave frequency and wave height, respectively. The waves are also classified in Fig. 7 with respect to their relative height and the relative water depth. It can be seen that the defined waves are not captured by linear wave theory and deep water approximations. Instead they are influenced by nonlinear effects as well as by a limited water depth. Especially the longest waves are significantly influenced by bottom effects.

TABLE 3: WAVE PARAMETERS USED FOR THE RAOS

$\lambda[m]$	$\omega[rad/s]$	$H[m]$
1.840	5.788	0.0286
2.386	5.065	0.0429
2.871	4.581	0.0428
3.540	4.061	0.0571
4.680	3.398	0.0856
6.000	2.844	0.1200

4.5 Implementation of the surge motions

In order to investigate the influence of the surge motion on the heave and pitch motions within the experimental setup, the suspension system of the experiments is abstracted and modelled instead by a simple spring which is connected to the center of gravity of the ship and a fixed point in space. This allows the ship to surge although the spring stiffness is restricting the magnitude of the surge motions. From the experiments, the spring stiffness is not documented but its value is approximated by comparing the simulated surge amplitude to the experimental one. In all simulations the spring constant c_s is chosen to be $100\frac{N}{m}$ and the resulting spring force F_s is defined by

$$F_s = c_s \Delta x \tag{6}$$

with

$$\Delta x = ||\vec{x}_{env} - \vec{x}_{cog}||_2 - l_r \ .$$

The relaxation length l_r allows to vary the distance between the spring's mounting locations $\vec{x}_{env}$ and $\vec{x}_{cog}$ without changing the

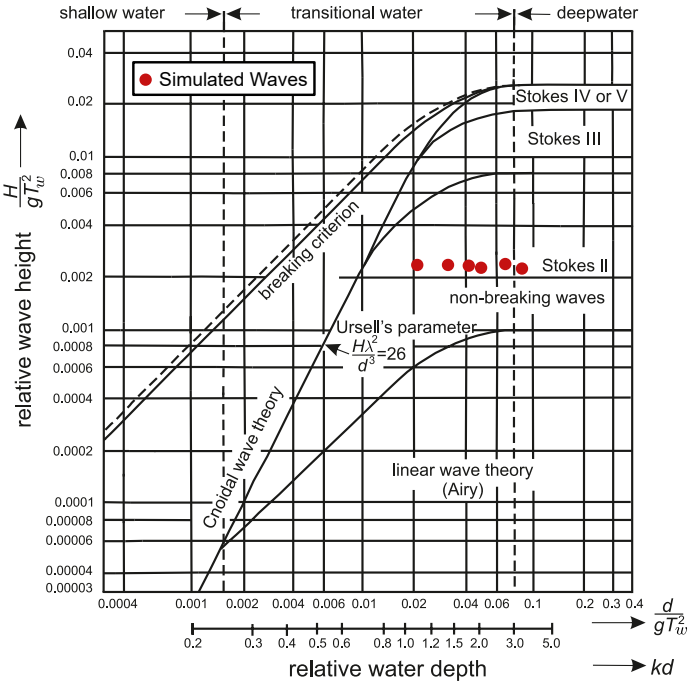

FIGURE 7: OVERVIEW OF APPLICABILITY OF WAVE THEORIES CF. [25].

effective elongation. So, with a proper distance between $\vec{x}_{env}$ and $\vec{x}_{cog}$ at the ship's moving center of gravity, the vector of the spring force is only slightly varying despite the ship's heave motion. In order to allow a decay of the spring eigen frequency in feasible time scales, a damping term

$$F_d = b_s \dot{x} \tag{7}$$

is additionally included in the x-direction. The damping constant b_s is chosen very small, leading to a damping factor D_s

$$D_s = \frac{b_s}{2\sqrt{c_s m_{ship}}}$$

of only 0.05.

5. RESULTS

Before conducting the simulations, the temporal and spatial discretization was reassessed to assure a sufficient resolution of the mesh and the time integration. As the chosen time steps sizes are reduced by one order of magnitude compared to recommendations of the *ITTC* (cf. Sect. 4), errors resulting from the temporal discretization should be sufficiently small. With respect to the spatial resolution, common references and guidelines are considered which are confirmed through refinement studies during the development of the numerical setup.

Wave elevation measurement The computation of the RAO requires, besides the ship's response, the accurate wave amplitude to be measured. In several studies [13, 14, 23] the wave elevation is directly measured within the simulation, although this approach has some shortcomings. First, the measurement location is not

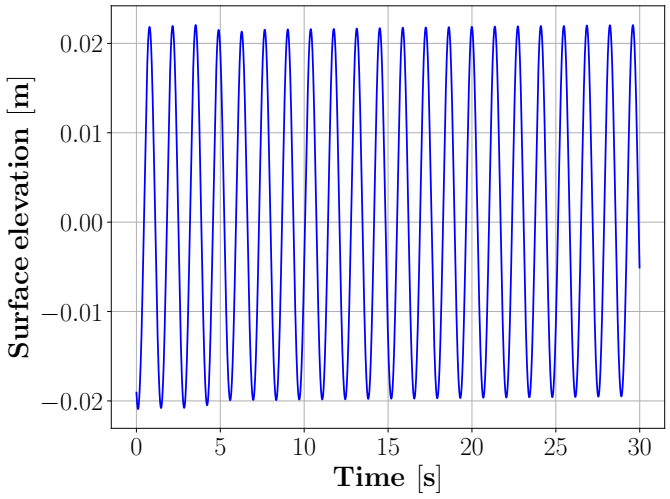

FIGURE 8: EXEMPLARY TIME SERIES OF THE SURFACE ELEVATION AT THE INITIAL POSITION OF THE CT'S CENTER OF GRAVITY

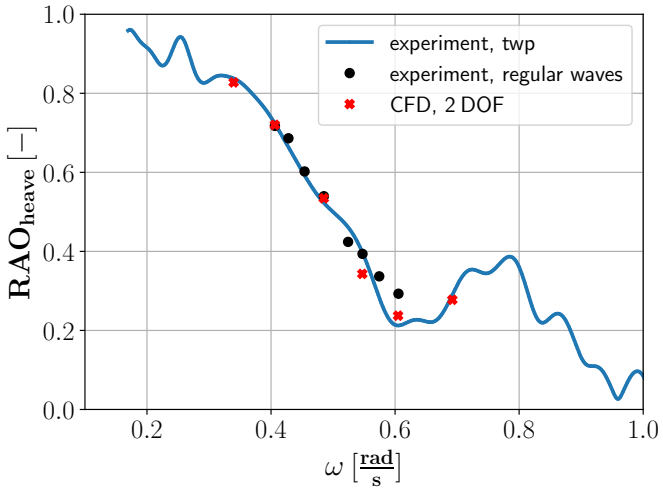

FIGURE 9: RAOS OF THE SHIP'S HEAVE MOTION WITH SUPPRESSED SURGE MOTION

the same like the reference position for the ship response, which is usually the center of gravity. Secondly, the ship motions lead to radiation of waves that influence the undisturbed regular wave. Particularly to circumvent the latter effect, all wave amplitudes are measured in a separate simulation. These simulations share the same setup and background mesh like the actual simulations but the overset mesh together with the ship geometry is removed to solely simulate the undisturbed wave. Moreover, the wave probe can be directly placed at the initial position of center of gravity of the ship. In Fig. 8, the time history of the surface elevation ζ at such a wave probe is shown for the wave with $\lambda = 2.871m$. For the determination of all the wave amplitudes, only the last three periods are considered by averaging the span between the maxima and minima:

$$A_w = \frac{1}{2}\frac{\sum_{i=n-2}^{n} \zeta_{max,i} - \zeta_{min,i}}{3}$$

Response Amplitude Operator A ship's response to waves is usually related to the exciting wave amplitude, which gives the Response Amplitude Operator (RAO) allowing comparisons independent of the specific wave amplitude. Therefore, the motion amplitudes which are presented along the paper are given as the RAO scaled from model to real ship size via Froude scaling laws. The specific RAOs are defined by:

$$RAO_{heave} = \frac{A_3}{A_w}$$

$$RAO_{pitch} = \frac{A_5}{A_w},$$

wherein A_3 and A_5 correspond to the ship's heave and pitch amplitude and A_w to the measured wave amplitude.

5.1 Ship response with suppressed surge motion

The standard approach to model the ship in head waves is to prevent any surge motion / lateral motion of the ship by applying an external forces that compensates the sum of all other forces in that direction. With this approach, all the waves defined in Tab. 3 are simulated with the CT free to heave and pitch.

Figure 9 depicts the simulated ship responses and also shows experimental results obtained by a TWP, which implies linear wave response behaviour, as well as results for the experimental counterparts of the simulated Stokes-II waves. The agreement between CFD and experimental results is good. Especially the CFD results for the longer waves almost perfectly match the experimental results. The simulated responses in shorter waves are still in an acceptable range of accuracy, although the predicted heave response is underestimated compared to the experimental results for the single regular waves.

The outcome for the pitch response of the ship is visualized in Fig. 10. In contrast to the results for the heave response, the highest deviations in the pitch RAO are found for the longest simulated waves. So, the pitch response at the peak of the RAO at around $\omega = 0.5$ is overestimated while the shortest simulated waves lead to small deviations when compared to the experimental results. Thus, the CFD simulations are not only able to cover the overall characteristics of the measured pitch RAO as well as the heave RAO but also reach an adequate accuracy level.

5.2 Ship response with surge motion

To allow surge motions, a spring force is applied lateral direction to the ship, whose initial elongation is determined by the average wave force, which can be obtained from the previous, constrained simulations. As the spring force almost ideally acts in longitudinal x-direction without inducing any additional moment, its influence is restricted to the surge motion of the ship. Therefore, any differences to the simulations with only two degrees of freedom should originate from the additional surge motion. In Fig. 11 an exemplary time series of the heave, pitch and surge motion of the chemical tanker exposed to a wave ($\lambda = 3.54m$) is shown. The heave and pitch oscillations quickly reach a constant amplitude, while the oscillating surge motion is superimposed by an additional decaying transient. This transient originates from

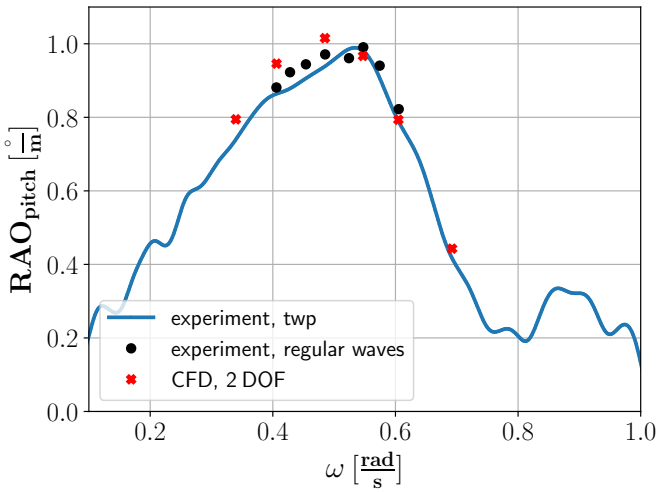

FIGURE 10: RAOS OF THE SHIP'S PITCH MOTION WITH SUPPRESSED SURGE MOTION

the coupling with the spring whose eigen oscillation decays according to the theory of a 1-D mass-spring system with $\propto e^{D_s \omega_s t}$. Therein, D_s is the damping factor of the spring-system and ω_s the respective eigen frequency. The amplitudes of the heave and pitch motion are evaluated and presented as RAOs in Fig. 12 which also contains the results from the simulation with the restricted surge motion. For the heave motion, there is almost no difference between the two setups. For all the simulated waves, the heave RAO is nearly the same, indicating that the surge motion has a negligible influence on the heave motion even for the longer waves with a more pronounced surge motion. In contrast to that, the pitch motion is significantly influenced by the surge motion. This is shown in Fig. 13 where the computed pitch RAOs with surge motion clearly differ from the ones computed with the restricted surge motion. The differences are small for the shortest waves as the surge amplitude is small itself. With increasing wave length, the differences increase towards the peak of the pitch RAO. The change in the RAO leads to an higher agreement between the CFD results and the experimental results for the longer waves. This suggests that modelling the effect of the surge motion can increase the accuracy of the predicted pitch motion, most notably in the frequency range around the peak of the pitch RAO.

5.3 Assessment of surge motion effect with Boundary Element Method

In order to critically scrutinize the findings from the CFD simulations, the open-source BEM solver *NEMOH* [15–17] is utilized to assess the effect of the surge motion with a model of reduced complexity. *NEMOH* is based on the well-established Boundary Element Method which solves the potential equation in the frequency-domain for fluid-body interactions in linear waves. For a detailed description of the method and the solver refer e.g to [33, 34]. In our case, all hydrodynamic forces, the added mass matrix and hydrodynamic damping matrix are computed for all six degrees of freedom with the help of *NEMOH*. However, the motion equations which directly lead to the RAOs for all degrees of freedom are transferred to a constrained linear optimization problem, that is solved externally. In accordance to the procedure in the CFD solver, all motions, except the allowed pitch, heave and potentially surge motion, are restricted to zero without restricting the forces in these directions. A difference to the CFD setup in three degrees of freedom is that the surge motion corresponds to the natural surge motion without an additionally applied spring force. In Fig. 14, the RAO for heave, pitch and surge (2 DOF and 3 DOF) computed with the elaborated approach are compared to the experimental RAOs. It can be seen that the BEM results match the experimental results quite well, especially for the heave motion. Most notably, the difference in the heave motion for the 2-DOF case and the 3-DOF case is vanishing small which directly confirms the findings from the CFD results. Moreover, the change of the pitch RAO when allowing surge motions is also following the trend from Fig. 13. For short waves, there is almost no effect of the surge motion on the pitch motion, while for longer waves the influence increases. The highest deviations are present at the peak of the pitch RAO. Here, the restricted surge motion leads to a higher peak and higher overall values of the pitch response in long waves. So for both, heave and pitch motion, a high agreement between CFD and BEM results is identifiable supporting the initial findings in Sect. 5.2. Considering the high agreement between BEM and experimental results and the easier applicability of the BEM compared to CFD, BEM might seem like the favorable tool for computing RAOs in head waves of moderate steepness. However, the accuracy of the BEM is likely to decrease for oblique or steeper waves where viscous and nonlinear effects become relevant that are not modelled by the standard BEM.

6. CONCLUSION

In this work, the motion response of a chemical tanker in regular head waves is assessed by means of CFD calculations and compared against results obtained from experiments. The numerical results with the standard setup, in which the ship is only free to heave and pitch, reveal reasonable agreement. In addition to that the numerical setup is critically assessed with respect to the restriction of the surge motion by utilizing a spring-system to model surge motions. By this, the influence of the surge motion on the heave and pitch motion is assessed and compared to BEM calculations. CFD and BEM consistently indicate a negligible influence on the heave motion but a significant influence on the pitch motion. Integrating the third degree of freedom for the surge motion of the ship leads to a smaller predicted pitch motion for long waves up to the peak of the CT's pitch RAO. According to these findings, the prediction accuracy for the pitch motion in head waves can be increased by including the influence of surge motions. Future investigations could aim for an assessment of the TWP-technique in CFD to significantly decrease the effort for obtaining the RAOs in regular waves.

ACKNOWLEDGMENTS

The authors gratefully acknowledge the scientific support and HPC resources provided by the German Aerospace Center (DLR). The HPC system CARA is partially funded by "Saxon

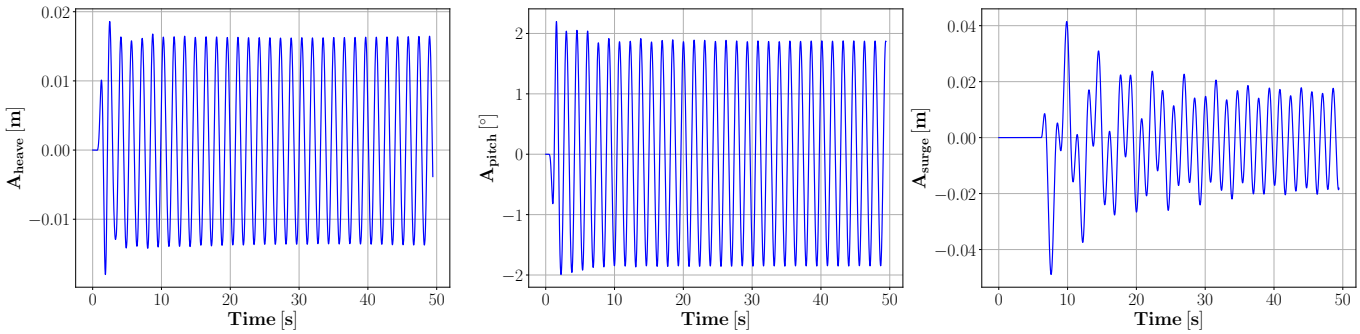

FIGURE 11: SHIP RESPONSE IN HEAVE, PITCH AND SURGE TO THE WAVE WITH $\lambda = 3.54m$

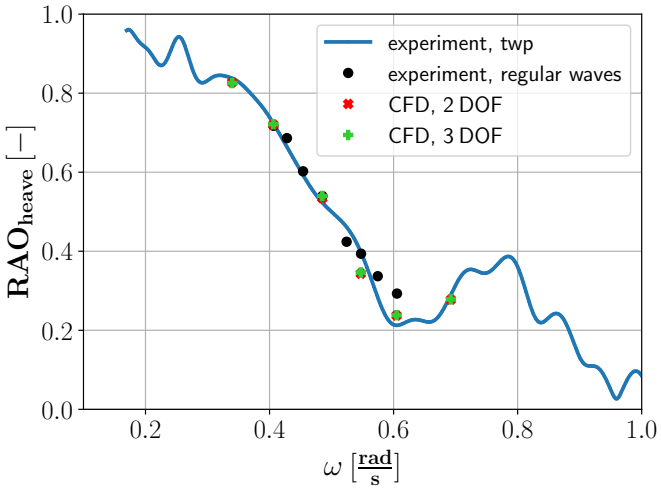

FIGURE 12: RAOS OF THE SHIP'S HEAVE MOTION INCLUDING SURGE MOTION

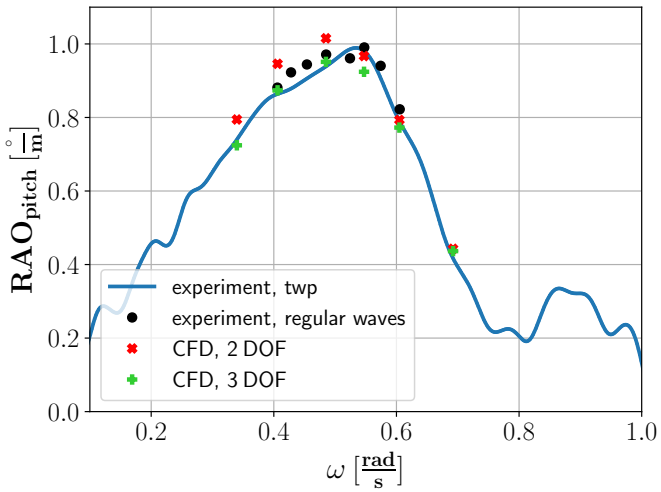

FIGURE 13: RAOS OF THE SHIP'S PITCH MOTION INCLUDING SURGE MOTION

State Ministry for Economic Affairs, Labour and Transport“ and „Federal Ministry for Economic Affairs and Climate Action”.

REFERENCES

[1] Hochkirch, Karsten and Mallol, Benoit. “On the importance of full-scale CFD simulations for ships.” *11th International conference on computer and IT applications in the maritime industries, COMPIT*. 2013.

[2] Terziev, Momchil, Tezdogan, Tahsin and Incecik, Atilla. “Scale effects and full-scale ship hydrodynamics: A review.” *Ocean Engineering* Vol. 245 (2022): p. 110496. DOI 10.1016/j.oceaneng.2021.110496.

[3] Hino, Takanori, Stern, Frederick, Larsson, Lars, Visonneau, Michel, Hirata, Nobuyuki and Kim, Jin. “Numerical Ship Hydrodynamics: An Assessment of the Tokyo 2015 Workshop.” *Lecture Notes in Applied and Computational Mechanics* (2021)DOI 10.1007/978-3-030-47572-7.

[4] Sanada, Yugo, Kim, Dong-Hwan, Sadat-Hosseini, Hamid, Stern, Frederick, Hossain, Md Alfaz, Wu, Ping-Chen, Toda, Yasuyuki, Otzen, Janne, Simonsen, Claus, Abdel-Maksoud, Moustafa, Scharf, Martin and Grigoropoulos, Gregory. “Assessment of EFD and CFD capability for KRISO Container Ship added power in head and oblique waves.” *Ocean Engineering* Vol. 243 (2022): p. 110224. DOI 10.1016/j.oceaneng.2021.110224.

[5] Peri, Daniele, Rossetti, Michele and Campana, Emilio F. “Design Optimization of Ship Hulls via CFD Techniques.” *Journal of Ship Research* Vol. 45 No. 02 (2001): pp. 140–149. DOI 10.5957/jsr.2001.45.2.140.

[6] Kim, Daejeong, Song, Soonseok and Tezdogan, Tahsin. “Free running CFD simulations to investigate ship manoeuvrability in waves.” *Ocean Engineering* Vol. 236 (2021): p. 109567. DOI 10.1016/j.oceaneng.2021.109567.

[7] Sadat-Hosseini, Hamid, Wu, Ping-Chen, Carrica, Pablo M., Kim, Ho, Toda, Yasuyuki and Stern, Frederick. “CFD verification and validation of added resistance and motions of KVLCC2 with fixed and free surge in short and long head waves.” *Ocean Engineering* Vol. 59 (2013): pp. 240–273. DOI 10.1016/j.oceaneng.2012.12.016.

[8] Hizir, Olgun, Kim, Mingyu, Turan, Osman, Day, Alexander, Incecik, Atilla and Lee, Yongwon. “Numerical studies on non-linearity of added resistance and ship motions of

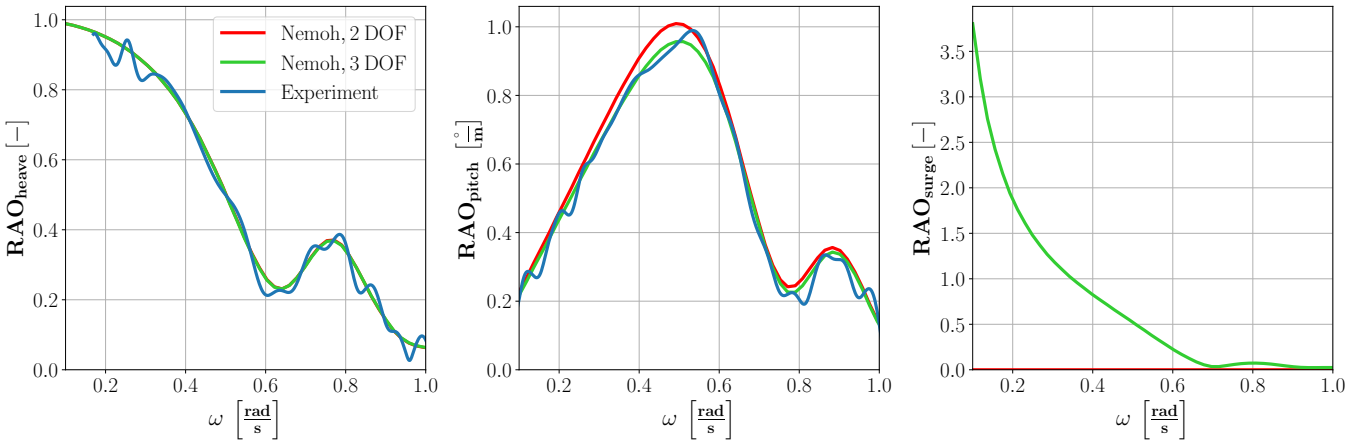

FIGURE 14: RAOS FOR THE HEAVE, PITCH AND SURGE MOTION PREDICTED WITH NEMOH WITH NATURAL SURGE MOTION (3 DOF) AND SUPPRESSED SURGE MOTION (2 DOF)

KVLCC2 in short and long waves." *International Journal of Naval Architecture and Ocean Engineering* Vol. 11 No. 1 (2019): pp. 143–153. DOI 10.1016/j.ijnaoe.2018.02.015.

[9] Siemens Digital Industries Software. "Simcenter STAR-CCM+ User Guide v. 2021.1." (Siemens 2021).

[10] Wang, Shan, Klein, Marco, Ehlers, Sören, Clauss, Günther and Guedes Soares, C. "Analysis of the Behavior of a Chemical Tanker in Extreme Waves." *Journal of Marine Science and Application* (2024)DOI 10.1007/s11804-024-00508-0.

[11] Ley, Jens and el Moctar, Ould. "A Comparative Study of Computational Methods for Wave-Induced Motions and Loads." *Journal of Marine Science and Engineering* Vol. 9 No. 1 (2021): p. 83. DOI 10.3390/jmse9010083.

[12] Simonsen, Claus D., Otzen, Janne F., Joncquez, Soizic and Stern, Frederick. "EFD and CFD for KCS heaving and pitching in regular head waves." *Journal of Marine Science and Technology* Vol. 18 No. 4 (2013): pp. 435–459. DOI 10.1007/s00773-013-0219-0.

[13] Niklas, Karol and Pruszko, Hanna. "Full scale CFD seakeeping simulations for case study ship redesigned from V-shaped bulbous bow to X-bow hull form." *Applied Ocean Research* Vol. 89 (2019): pp. 188–201. DOI 10.1016/j.apor.2019.05.011.

[14] Tahsin Tezdogan, Atilla Incecik and Osman Turan. "Full-scale unsteady RANS simulations of vertical ship motions in shallow water." *Ocean Engineering* Vol. 123 (2016): pp. 131–145.

[15] A. Babarit, G. Delhommeau. "Theoretical and numerical aspects of the open source BEM solver NEMOH." *Proc. of the 11th European Wave and Tidal Energy Conference (EWTEC2015)*.

[16] R. Kurina, G. Ducrozet. "Computation Of Second-Order Wave Loads On Floating Offshore Wind Turbine Plattforms in Bi-Chromatic Bi-Directional Waves Using Open-Source Potential Flow Solver Nemoh." *18èmes Journées de l'Hydrodynamique*. URL https://jh2022.sciencesconf.org/420480/document.

[17] Kurnia, R., Ducrozet, G. and Gilloteaux, J.-C. "Second Order Difference- and Sum-Frequency Wave Loads in the Open-Source Potential Flow Solver NEMOH." *Volume 5A: Ocean Engineering*. 2022. American Society of Mechanical Engineers. DOI 10.1115/OMAE2022-79163.

[18] Günther F. Clauss and Jan Bergmann. "Gaussian wave packets — a new approach to seakeeping testsof ocean structures." *Applied Ocean Research* Vol. 8 No. 4 (1986): pp. 190–206. DOI 10.1016/S0141-1187(86)80036-0.

[19] P. Roux de Reilhac, F. Bonnefoy, J.M. Rousset and P. Ferrant. "Improved transient water wave technique for the experimental estimation of ship responses." *Journal of Fluids and Structures* Vol. 27 No. 3 (2011): pp. 456–466. DOI 10.1016/j.jfluidstructs.2011.01.002. URL https://www.sciencedirect.com/science/article/pii/S0889974611000053.

[20] Gopala, Vinay R. and van Wachem, Berend G.M. "Volume of fluid methods for immiscible-fluid and free-surface flows." *Chemical Engineering Journal* Vol. 141 No. 1-3 (2008): pp. 204–221. DOI 10.1016/j.cej.2007.12.035.

[21] Muzaferija S., Peric M., Sames P., Schelin T. "A two-fluid NavierStokes solver to simulate water entry." *Twenty-Second Symposium on Naval Hydrodynamics, 1998*.

[22] Klaij, C. M., Hoekstra, M. and Vaz, G. "Design, analysis and verification of a volume-of-fluid model with interface-capturing scheme." *Computers & Fluids* Vol. 170 (2018): pp. 324–340. DOI 10.1016/j.compfluid.2018.05.016.

[23] Huang, Songxing, Jiao, Jialong and Chen, Chaohe. "CFD prediction of ship seakeeping behavior in bi-directional cross wave compared with in uni-directional regular wave." *Applied Ocean Research* Vol. 107 (2021): p. 102426. DOI 10.1016/j.apor.2020.102426.

[24] Subrata K. Chakrabarti (ed.). *Handbook of offshore engineering*, volume ii ed. Elsevier, Amsterdam and Heidelberg (2008).

[25] Clauss, Günther, Lehmann, Eike and Östergaard, Carsten. *Offshore Structures*. Springer London, London (1992). DOI 10.1007/978-1-4471-3193-9.

[26] John D. Fenton. "A Fith-Order Stokes Theory For Steady Waves." *Journal of Waterway, Port, Coastal and Ocean Engineering* No. 111 (1985).

[27] John D. Fenton. "Nonlinear Wave Theories." *The Sea, Ocean Engineering Science* No. 9 (1990).

[28] Siemens Digital Industries Software. "Simcenter STAR-CCM+, version 2021.1." (Siemens 2021).

[29] Versteeg, Henk K. *An introduction to computational fluid dynamics: The finite volume method*, 2nd ed. Pearson/Prentice Hall, Harlow [u.a.] (2011).

[30] Stern, Frederick, Yang, Jianming, Wang, Zhaoyuan, Sadat-Hosseini, Hamid, Mousaviraad, Maysam, Bhushan, Shanti and Xing, Tao. "Computational ship hydrodynamics: Nowadays and way forward." *International shipbuilding progress* Vol. 60 No. 1-4 (2013): pp. 3–105. DOI 10.3233/ISP-130090.

[31] "ITTC Quality System Manual - Recommended Procedures and Guidelines: Practical Guidelines for Ship CFD Applications."

[32] Versteeg, H. K. and Malalasekera, W. *An introduction to computational fluid dynamics: The finite volume method*, 2nd ed. Pearson/Prentice Hall, Harlow (2007).

[33] el Moctar, Bettar Ould, Schellin, Thomas E. and Söding, Heinrich. *Numerical Methods for Seakeeping Problems*. Springer International Publishing, Cham (2021). DOI 10.1007/978-3-030-62561-0.

[34] G. Delhommeau. "Amelioration des Performances des Codes de Calcul de Diffraction-Radiation au Premier Ordre." *2èmes Journees de L'Hydrodynamique*.